Pertanika J. Sci. & Technol. 32 (6): 2769 - 2796 (2024)

PERTANIKA JOURNALS

SCIENCE & TECHNOLOGY

Journal homepage: http://www.pertanika.upm.edu.my/

Review Article

A Comprehensive Review of State-of-the-art Optical Methods for Methane Gas Detection

Sayma Khandaker, Nurulain Shaipuzaman, Md Mahmudul Hasan, Mohd Amir Shahlan Mohd Aspar and Hadi Manap*

Faculty of Electrical and Electronics Engineering Technology, Universiti Malaysia Pahang Al-Sultan Abdullah, 26600 Pekan, Pahang, Malaysia

ABSTRACT

Methane (CH_4), a potent greenhouse gas, significantly contributes to climate change and global warming. Its impact over 100 years surpasses carbon dioxide (CO_2) by 28 times. Addressing methane emissions, particularly from oil and gas production activities such as transmission pipelines, is imperative. One promising avenue is the development of reliable sensors to detect and mitigate methane leaks and prevent hazardous issues. Optical-based methods present notable advantages, including versatility and remote operation, making them pivotal in this endeavor. This review article provides a concise overview of optical-based methane identification technologies, encompassing sensing materials, absorption spectra, operational mechanisms, and recent advancements. Potential perspectives are explored, and inferences from this assessment are also derived. Emphasizing the significance of optical fiber-based methane detection methods, the authors advocate for further research to support ongoing efforts and foster innovation in this critical area.

Keywords: Methane absorption spectra, methane detection, methane sensing materials, optical fiber sensor, optical methods

ARTICLE INFO

Article history:
Received: 31 January 2024
Accepted: 19 August 2024
Published: 25 October 2024

DOI: https://doi.org/10.47836/pjst.32.6.19

E-mail addresses:
saymakhandaker27@gmail.com (Sayma Khandaker)
ainnadhirah93@gmail.com (Nurulain Shaipuzaman)
mhasan.just@gmail.com (Md Mahmudul Hasan)
amirs@umpsa.edu.my (Mohd Amir Shahlan Mohd Aspar)
hadi@umpsa.edu.my (Hadi Manap)
* Corresponding author

INTRODUCTION

The main component of natural gas is methane (CH_4). It is an odorless, colorless gas with melting and boiling points of -183°C and -164°C, respectively. Its high heating value and excellent igniting properties make it a popular fuel for heating and power generation worldwide. Compared to coal,

ISSN: 0128-7680
e-ISSN: 2231-8526

CH_4 has a higher calorific value and produces fewer toxic and harmful compounds when burned, making it an essential resource for economies aiming to reduce carbon emissions. Due to its lower production costs and reduced combustion-related CO_2 emissions, it is increasingly replacing coal, particularly in the US power sector (Jaramillo et al., 2008).

However, the utilization of CH_4 and its release into the atmosphere have serious implications. After CO_2, CH_4 is the second most common greenhouse gas. Its potential to contribute to global warming is roughly thirty times higher per molecule than that of CO_2. Since the onset of industrialization, there has been a significant increase in the quantity of methane in the atmosphere, reaching as high as 1800 parts per billion (ppb) in 2016 (Turner et al., 2019), compared to less than 800 parts per billion at the beginning of the nineteenth century.

Waste disposal facilities, livestock waste disposal systems, coal extraction, petrochemical exploration, electricity transformers, and gas and oil transportation and manufacturing facilities are the primary human causes of emissions responsible for this rise. Additionally, if the concentration of methane gas in an enclosed area exceeds 5% to 15%, it may ignite and cause an explosion (Stocker et al., 2014).

Given its abundant supply and relatively safe combustion process, natural gas is expected to be utilized extensively despite its negative environmental implications (Tran & Fowler, 2020). The World Health Organization (WHO) claims that CH_4 may remain in the atmosphere for a maximum of 12 years before being gradually depleted by molecules such as OH radicals, which pose a significant environmental risk when discharged into the atmosphere (Lawrence, 2006).

Over the past two centuries, the atmospheric concentration of methane has more than doubled. This significant increase is primarily due to the exponential rise in human activity, which elevates atmospheric methane concentration through various emission pathways. Methane is a crucial component of natural gas in the atmosphere and is also found in adjacent regions of the world's layers. It is generated by the decomposition of animals, plants, or microorganisms inhabiting oceans, lakes, and other bodies of water.

Approximately 36% of the total methane volume originates from naturally occurring wetland emissions produced by termites and the ocean. About 64% of all methane emissions come from human activities, including landfills, paddy fields, agriculture, and livestock digestion, as depicted in Figure 1 (Vasiliev et al., 2014). Nevertheless, depending on the source, methane emission numbers can differ considerably.

The Conference Board of Canada found that 8.5% of Canada's greenhouse gas emissions are attributed to methane leakage from wells and equipment (Bachu, 2017). According to Olmer et al. (2019), methane emissions from transporting liquefied natural gas account for over five percent of the 932 million tons of CO_2 equivalent emissions worldwide. Ingraffea et al. (2020) discovered that Pennsylvania's oil and gas wells emit

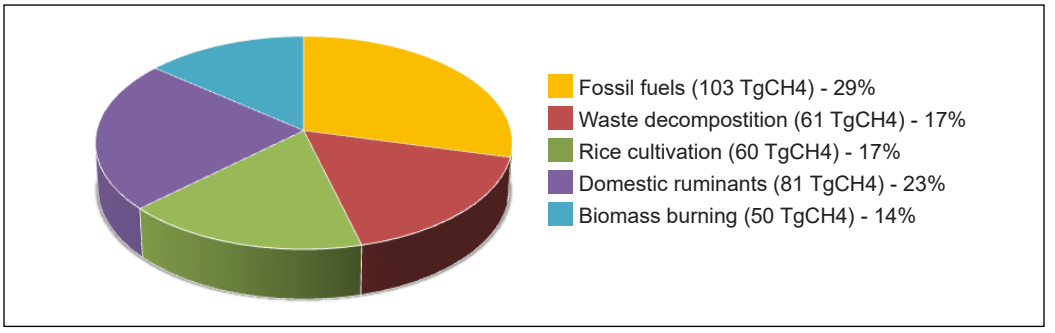

Figure 1. Individual sources of the world's total emissions of methane

an average of 55,600 tons of methane annually. The shale gas basins in northern British Columbia are estimated to leak 75,000 metric tons of methane annually (Wisen et al., 2020). Formisano et al. (2004) revealed methane in the Martian atmosphere. The planet's concentration ranges from 0 to 30 parts per billion by volume (ppbv), with an average of 10 ± 5 ppbv. The measurements were taken with the Mars Express spacecraft's planetary FTIR spectrometer. This gas is expected to increase the likelihood of uncovering evidence of life on Mars. Methane in the Martian atmosphere decomposes rapidly through various processes. Therefore, large clouds of this gas in Mars' northern hemisphere suggest continuous methane emissions. Methane is also used in small quantities for medical diagnosis. When the stomach microbiota is imbalanced, methane can be detected in the air, indicating irritable bowel syndrome. Consequently, methane is released into the bloodstream and travels to the lungs.

However, numerous methods are available for detecting CH_4 nowadays, each with benefits and drawbacks. Optical fiber-based methane detection methods stand out for their remote operation, deployment versatility, high sensitivity to low concentrations, real-time monitoring capabilities, minimal interference, and cost-effectiveness, making them ideal for continuous and reliable methane surveillance. Unfortunately, detecting methane at leak-relevant quantities with these methods using widely deployable, reasonably priced equipment over long distances and/or wide geographic areas remains challenging. Due to their low polarizability, this difficulty stems from the inherently low reactivity of CH_4 molecules compared to other frequently researched gas molecules, such as H_2, CO_2, and CO.

This article provides an in-depth review of a wide range of commonly used optical fiber-based methane detection sensors, including information on their performance characteristics and current developments to enhance sensitivity, selectivity, response and recovery times, and long-term stability. It also meticulously analyzes the challenges and limitations associated with these sensors. Future research directions, including materials and optical sensor advancements, are explored to guide the development of more reliable and efficient methane detection systems.

METHANE SENSING MATERIALS

Depending on the surrounding gas environment, gas-sensing materials can modify their electrical, optical, or auditory properties. This article will compile the most recent research on CH_4 sensing materials in this domain, focusing on five categories: metal oxides, supramolecular materials, carbon-based substances, conductive polymers, and metal-organic frameworks. The sensing mechanism and effectiveness of each category will be explained. Additionally, the suitability and feasibility of utilizing diverse sensing materials on the platforms above and mechanisms will be compiled in Table 1. Table 2 also offers an overview of the CH_4 sensing capabilities of various materials. The ranges for response time, temperature requirements, and detection limits have been compiled based on the highest and lowest values from published studies. Materials for highly specific and reversible CH_4 sensing are continuously under investigation, unlike other gas sensors, including NH_3, H_2, and others. Therefore, the assessment of selective and reversible changes in these sensors is typically minimal or moderate, as listed in Table 2. The deposition of the sensing materials typically occurs in the formation of a polycrystalline layer or film onto a substrate that incorporates heating as well as embedded electrodes (Figure 2).

Table 1
Summary of the materials used for CH_4 sensing across various platforms and techniques (Hong et al., 2020)

Platform	Techniques		
	Electrical	Optical	Mass
Optical Fiber	-	1,3,4,5	-
Chemi-resistive	1,2,3	-	-
SAW/QCM	1	-	3,4,5

Note. 1: Metal-oxide; 2: Carbon; 3: Conducting polymer; 4: Supramolecular and 5: Metal-organic framework

Table 2
An overview of the various materials' characteristics for detecting CH_4 (Hong et al., 2020)

Material	Temperature of Operation	Time of Response (s)	Sensing Reversible Nature	Selection Level	Detection Threshold (ppm)
Metal-Oxide	25ºC–900ºC (normally > 150ºC)	10^0–10^2	Minimum-Medium	Minimum-Medium	10^0–10^3
Carbon	Room Temperature - 450ºC	10^1–10^2	Minimum-Medium	Minimum-Medium	10^1–10^4
Conducting Polymer	Room Temperature	10^1–10^2	Minimum-Medium	Minimum-Medium	10^2–10^3
Supramolecular	Room Temperature	10^1–10^2	Minimum-Medium	Minimum-Medium	10^1–10^4
Metal-organic Structure	Room Temperature	10^1–10^2	Medium-Maximum	Medium	10^4–10^5

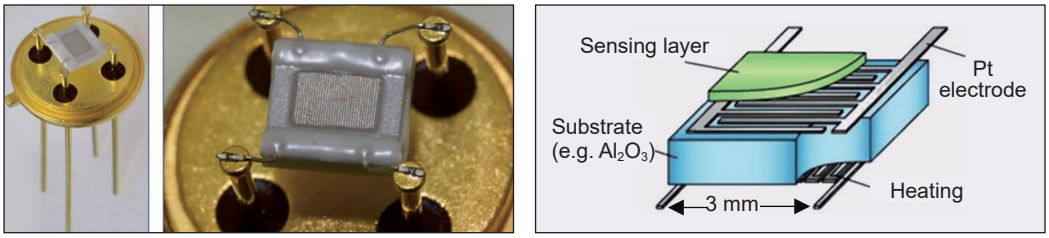

(a) (b)

Figure 2. (a) A graphical representation; and (b) snapshots of an illustrative sensing material, taken from (Tiemann, 2007)

METHANE ABSORPTION SPECTRA

The Lambert-Beer rule is the basis of optical gas detection using absorption spectrum analysis in Equations 1 and 2.

$$I(\lambda) = I_0(\lambda) \exp[-a(\lambda, C).L]\, a[cm^2] \quad [1]$$

$$I(\lambda) = I_0(\lambda) \exp[-\alpha(\lambda, C).L]\, \alpha[ppm.cm^2] \quad [2]$$

Where I is the amount of light transmission through the gas-filled medium; I_0 is the brightness of the incident light on the medium; C is the concentration; a, α is the coefficient of absorptions; and L is the optical path length.

The Pacific Northwest National Laboratory, part of the US Department of Energy (DOE), provides quantitative gas spectra, which can be determined using the HITRAN database (Rothman et al., 2009). Optical approaches for detecting methane rely on its infrared absorption properties. The absorption spectrum of methane, displayed in Figure 3,

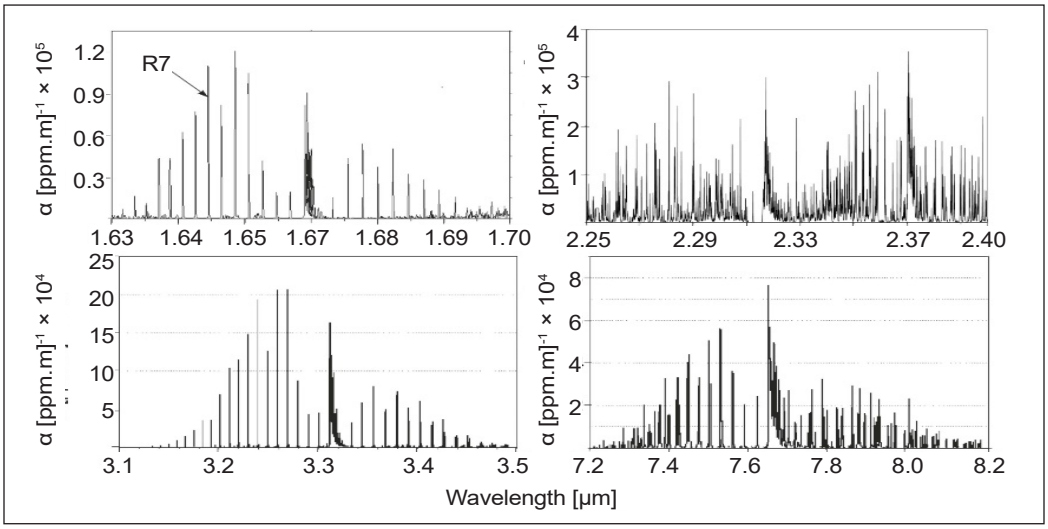

Figure 3. Methane absorption spectra (Adapted from Kwaśny & Bombalska, 2023)

shows that the strongest bands occur within the zone of deformation vibrations, followed by valence vibrations; these are weaker in the overtone spectrum.

There are numerous absorption lines for methane in the 1.63–1.69 μm range, with a composite absorption cross-section of 5.13 × 10^{-20} cm^2, making them highly influential. However, there are bands of carbon dioxide with an overall absorption of 4.95 × 10^{-23} cm^2 and water with an overall absorption of 4.34 × 10^{-23} cm^2 (Kwaśny & Bombalska, 2023). It is important to carefully select methane absorption lines to avoid interference from these absorbers. Figure 4 illustrates the selection of relevant bands for investigation, as well as the proximity of CH_4 and H_2O absorption lines to each other. It effectively operates immersion cells at lower pressures of 50–100 hPa to enhance spectral resolution and line separation and reduce half-width. Cooled detectors are unnecessary for instruments operating in the NIR region (0.8–2.5 μm) due to their expense.

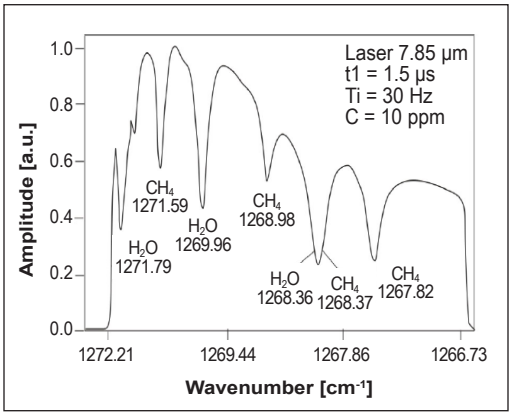

Figure 4. Atmospheric transmission spectrum with methane (Kwaśny & Bombalska, 2023)

METHANE GAS DETECTION BASED ON OPTICAL METHODS

Gas-detecting applications can represent a wide range of gas concentrations, generally indicated as a volumetric ratio in the air or another matrix. Since most gases behave as ideal gases to a large extent at normal temperatures and pressures, the molar concentration in the matrix is also identical or nearly equal (Hodgkinson & Tatam, 2013). An example of methane, which has multiple applications requiring measurement over a range of concentrations, can be used to illustrate gas concentrations. Table 3 provides a summary of several examples. Concentrations can be expressed as % volume, ppt, ppm, or ppb.

Different approaches now exist for identifying methane in the air, depending on whether the measurement is conducted in a laboratory, where samples are analyzed under stationary conditions, or outdoors, where continuous observation is performed. Various sensors can detect methane, including optical, pyroelectric, semiconducting metal oxide, electrochemical, and calorimetric sensors.

Thermal Conductivity Detector is one of the earliest sensors used to assess the composition of gas mixtures. This method involves detecting changes in the thermal conductivity of a carrier gas resulting from alterations in its chemical structure. The sensor is an imbalanced Wheatstone bridge consisting of two or four thermistors heated by current passing through them. High sensitivity, a linear response over a broad measurement range,

Table 3
Methane detection application that demonstrates the requirement for gas measurement across a range of concentrations (Hodgkinson & Tatam, 2013)

Execution	Major concerns	Desired concentration spectrum	Reference
Process monitoring: gas quality, i.e., the composition of natural gas measured for regulatory purposes, metering and the alteration of custody	Accuracy to 'fiscal standards' (0.1%)	70–100% volume	Wild, 2000
Process monitoring: tracking the combustion process	Accuracy throughout a broad range of temperatures and pressures	0.1%–100% volume	Pyun et al., 2011
Process/environment: measurement of methane residue in a flare for the exchange of carbon	Consistency: 100 parts per billion. Methane background concentration: 1.8 ppm; higher near sources	100 ppb - 1000 ppm (plus a background level of 1 Accuracy e.g., to ±5%.8 ppm)	Kannath et al., 2011
Environment-based modeling: The 1.8 ppm methane background assessment	Compared with previous data. Accuracy of 0.1%– 5% of reading required	30 ppb - 3 ppm (plus a background level of 1.8 ppm)	Gardiner et al., 2010
Environment-based modeling: measuring methane flux using eddy covariance technology	Interaction at data rates higher than 10 Hz with local atmospheric eddy currents	5 ppb - 25 ppm (plus a background level of 1.8 ppm)	McDermitt et al., 2011
Safety: Cleaning gas pipelines to prevent explosions and make sure the pilot lights stay sparked	Accuracy, e.g., to ±5% volume at 50% volume	1%–100% volume	Agius et al., 2000
Safety: measurement of gas leakage in relation to the 4.9% volume lower explosive limit	Accurate at action points, e.g., 20% lower explosive limit (1% volume) for evacuation of buildings	0.1%–5% volume	Gao et al., 2013; Hodgkinson & Pride, 2010
Safety: where gas spills are located, usually outside	Dependable detection threshold of about 1 ppm	1–10000 ppm	Hodgkinson & Pride, 2010; Hodgkinson et al., 2006

and a straightforward design characterize this sensor. However, key disadvantages include a lack of discrimination and the need to maintain constant sensor temperature, gas flow rate, and reference conditions.

In catalytic combustion sensors, a catalytic combustion reaction occurs on the active element, while changes in humidity, pressure, and temperature are measured using a passive component as a reference. The sensor utilizes a Wheatstone bridge. Catalytic combustion sensors are currently used in pellistors and hot fibers. A flammable gas and air stream is directly exposed to a hot platinum fiber in pellistors. In addition to serving as a heating element and resistance thermometer, the platinum wire also acts as a catalyst

for combustion. When an electric current passes through the circuit, the platinum wire reaches a temperature range of 400 to 500°C, allowing the gas mixture to undergo catalytic oxidation (Kwaśny & Bombalska, 2023).

Optical sensor technologies have become increasingly popular in recent decades due to their inherent advantages over other sensing platforms. These benefits include sensing remotely, immunity to electromagnetic interference, eliminating electrical lines and contacts in combustible gaseous settings, and non-invasive measurement techniques (Shemshad et al., 2012). Several research investigations and review studies have focused on optical technique-based gas sensors (Shemshad et al., 2012; Wang & Wolfbeis, 2016). Optical gas sensors detect variations in electromagnetic waves or visible light when the analyte comes into contact with the receptor section. Absorption and scattering are the basic mechanisms optical gas sensors use to detect emissions. A visual representation of a functional optical gas sensor for methane is depicted in Figure 5. It consists of an optical spectrum detector, a tube that holds the tested gas sample, and a light source that produces mid-IR light.

Optical technologies offer numerous benefits, including the ability to test methane remotely and at very low concentrations, such as ppm, ppb, and ppt. However, a primary drawback is the overlap of water bands during absorption and the presence of other hydrocarbons.

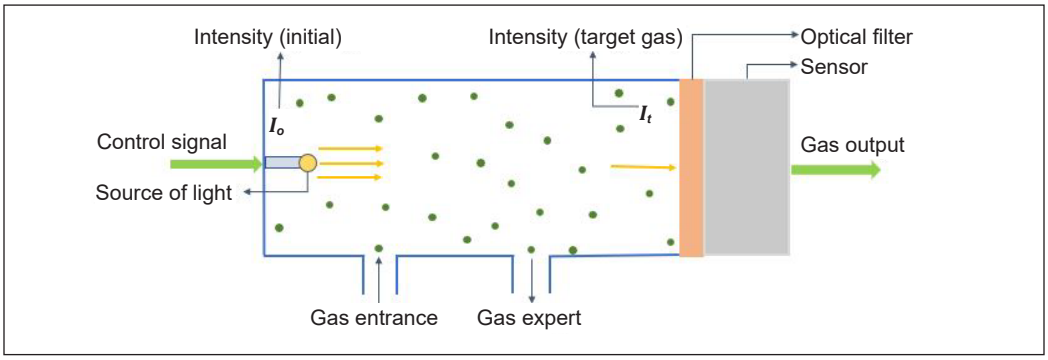

Figure 5. The working mechanism of an optical sensor for detecting methane

Tunable Diode Laser Absorption Spectroscopy

Tunable diode laser absorption spectroscopy (TDLAS) has been employed to detect temperature readings and gas concentrations in applications requiring high resolution, sensitivity, and precision. By adjusting the output wavelength of a diode laser, a single narrow linewidth laser can scan across distinct absorption paths to acquire measurements. Additionally, since absorption lines widen as pressure increases, high selectivity can be achieved at low pressures. Numerous researchers have developed methods for tracking trace gases. The TDLAS approach is a robust identification method that applies to all species absorbing infrared light and can produce a variety of laser wavelengths without requiring

additional equipment. Using a multiplexing method that pairs multiple laser outputs and utilizes a multipass cell, multiple gases can be monitored simultaneously. This approach responds quickly, typically in the range of 1 to 1000 µs, and is highly sensitive (Beckwith et al., 1987). However, limitations include the difficulty sustaining and employing this technology as a stand-alone system without routine technical repair and the restricted availability of laser initiation.

Various techniques utilize tunable diode laser spectroscopy to measure gas concentration and absorption, including wavelength, frequency modulation, and direct absorption spectroscopy. TDLAS achieves high resolution through a solitary channel of gas absorption across the emission wavelength of a narrow linewidth laser diode. The measurement can be self-referenced successfully by comparing the central peak absorption to the zero level on both sides of the spectrum. There are two main approaches for TDLAS: direct spectroscopy and wavelength modulation spectroscopy (WMS). Commercially available tools developed using these approaches include the SS2100 hydrogen sulfide analyzer (http://www.spectrasensors.com/asp/Site/Products/ByProduct/index.asp). Typically, a lock-in amplifier at the receiver is employed to recover the second harmonic of AC excitation to detect methane gas, as illustrated in Figure 6. Figure 7 displays the probable configurations of various demodulating waveforms for a single gas line.

The quality of the laser mode can significantly affect TDLAS. Achieving a high laser mode quality involves determining the pedestal temperature and driving current settings at which the laser produces strong, steady emission in a single mode at the targeted absorption

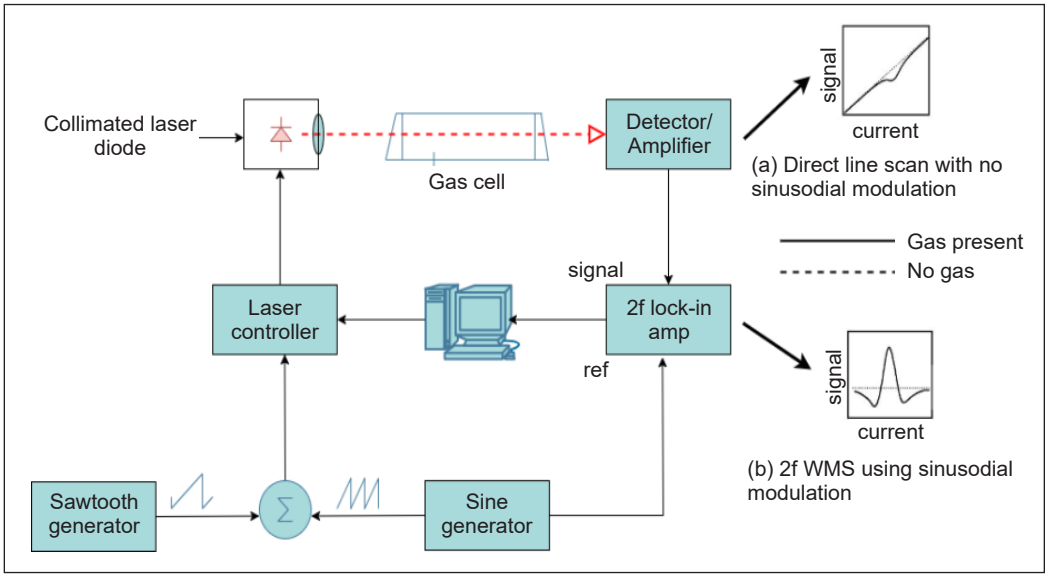

Figure 6. A laser diode is used in the conventional configuration of TDLAS to display observed signals as two objectives using a measure of laser drive current: (a) direct gas line scanning; or (b) second harmonic wavelength modulating spectroscopy (2f WMS)

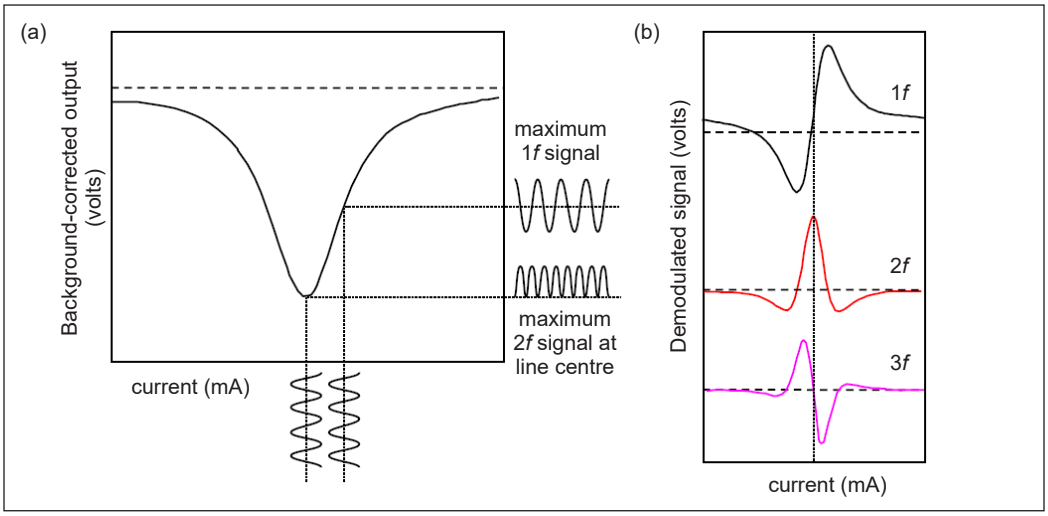

Figure 7. Various harmonic signals are generated in the WMS: (a) Background-corrected DC scan of a single gas line, with the RAM removed for clarity; and (b) The 1f, 2f, and 3f harmonics' form shifted for clarity, as a function of the current scan location. On the 1f signal, the RAM produces a slight but detectable dc offset extracted from (Hodgkinson & Tatam, 2013)

wavelength. However, this can be challenging as thermal cycling may cause changes in mode structure that alter the properties of the laser over time. Nevertheless, single-mode operation is preferred to minimize mode partition noise and remove interference from absorption signals of other modes with the primary absorption signal of the target species.

We have comprehensively reviewed recent publications on methane identification using TDLAS and compiled a summary of these findings in Table 4.

Table 4
Comparison measurements of performance for optical-based methane detection

Wavelength (μm)	Path	Response Time (s)	Minimum Detectable Concentration	Minimum Detectable Absorbance	Minimum Detectable Absorption Coefficient	Reference
2.3	72 m	137	0.487 ppm	Not stated	Not stated	Shao et al., 2019
1.65	80 mm	0.3	52 ppb	2.1×10^{-8} $cm^{-1}W/Hz^{1/2}$	1.455×10^{-21} cm^{-1}	Wei et al., 2021
1.684	20 cm	2	4.3 ppm	Not stated	Not stated	Hennig et al., 2003
1.6482	74 m	1.5–10	0.1 ppm	$4 - 8 \times 10^{-5}$	Not stated	Gurlit et al., 2005
1.654	252 m	2	20 ppb	Not stated	Not stated	Richard et al., 2002
8.03	76 m	1	1 ppb	4.6×10^{-5} $Hz^{-1/2}$	6.1×10^{-9} cm^{-1} $Hz^{-1/2}$	McManus et al., 2008

Non-dispersive Infrared

To compensate for the laser wavelength shift caused by heat in laser absorption spectroscopy, one of the most straightforward methods is the construction of broadband non-dispersive infrared (NDIR) sensors, which hold significant importance from a business standpoint. These sensors feature robust housing that serves as a gas flow measurement chamber, accommodating both a broadband light source and a combination detector. Figure 8 presents a visual representation of a basic NDIR sensor. Typically, two filters spanning a non-absorbed area are employed in the target channel and the reference channel, allowing the passage of emissions from a broadband source. Broadbands are employed for non-dispersive measurements. The two primary advantages of using micro bulbs in conventional NDIR sensors are their low cost and relatively high spectral emission.

Cuvettes with various optical path lengths are designed based on the volume of the concentrations and the absorption characteristics of the contaminants under investigation. Figure 9 shows an opto-pair (optoelectronic pair), an optical sensor. The method for distinguishing methane absorption in the opto-pair sensor is depicted in Figure 10. While the reference channel's optical filter transmits data within the 3.0–2.9 µm range, the working channel transmits in the range of 3.23 µm (Kwaśny & Bombalska, 2023).

A diffusion-type measurement cuvette filters light emitted by the radiation-emitting light source. Detectors operating in the absorption and reference bands separate it into two beams for analysis (Kwaśny & Bombalska, 2023). A spatial control network with up to 128 meters can be built using the RS-485 digital output. Its low drift and good measurement stability distinguish it from similar devices. The microprocessor inside the device generates pulses for the photosensitive sensor. Digital analysis is then used to measure the amplitudes of the signal pulses originating from amplifiers 4

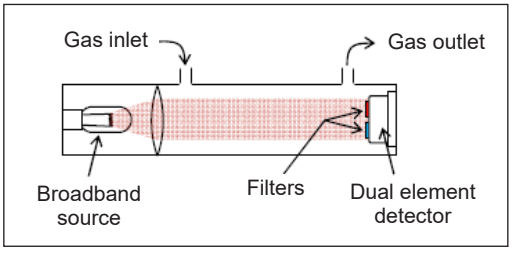

Figure 8. Conceptual illustration of a distinctive non-dispersive infrared gas sensor with optical path length, taken from (Hodgkinson & Tatam, 2013)

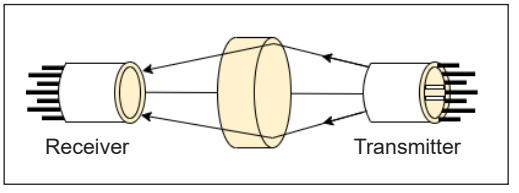

(a)

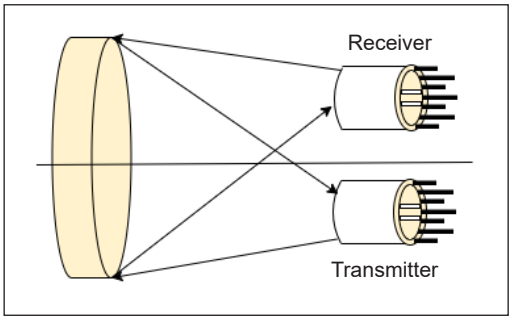

(b)

Figure 9. The notion of an opto pair (a) single radiation pass, (b) two radiation passes

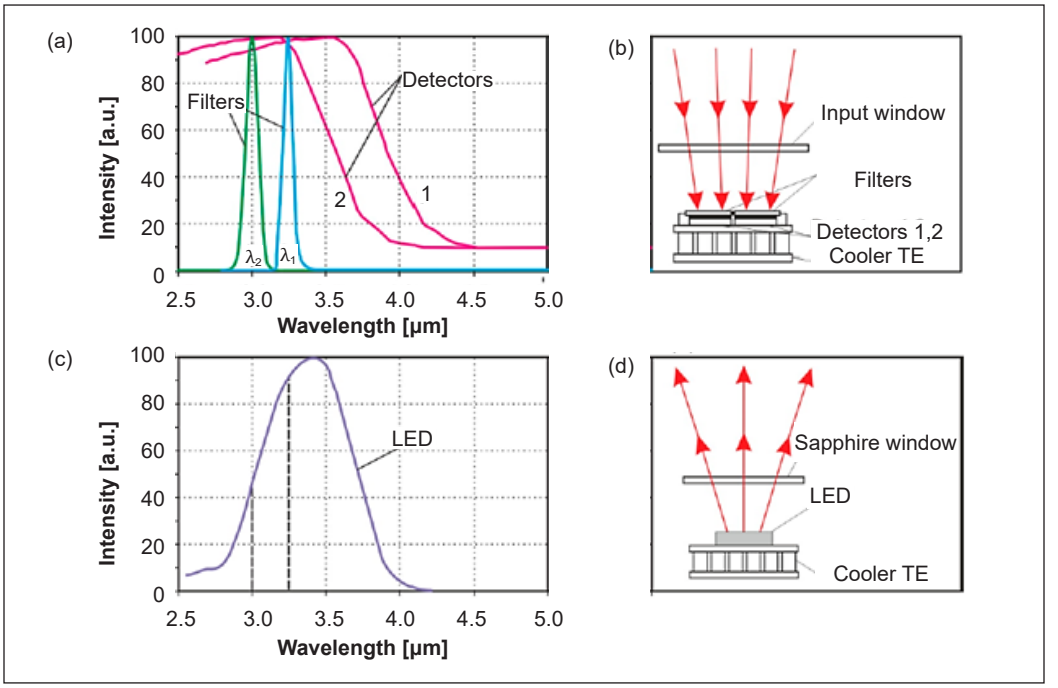

Figure 10. The opto-pair principle of methane measurement consists of: (a) filter transmittance and detector sensitivity; (b) detector block; (c) source emission spectrum; and (d) light source block. Adapted from Kwaśny & Bombalska, 2023

and 5 for the reference and working channels, respectively. The microprocessor controls the amplitude of the current, and the photodiode driver keeps it protected and stabilized at a predetermined level. The radiation emitted by the infrared photodiode covers the absorption bands of the examined gases, which are detected by detectors 1 and 2 in the absorption band and outside the band, respectively. Finally, the microprocessor computes the working and reference pulse amplitudes. Equation 3 is used to calculate their mathematical processing as well as the gas concentration.

$$C = -\ln\left(I_p - I_0\right)/L[\alpha(\lambda_p) - \alpha(\lambda_0)] \quad [3]$$

Where, L is the optical path length; I_p and I_0 are the operating channel's and reference's amplitude; and α is the coefficient of absorption at a specific wavelength.

Operating in temperatures ranging from -20 to 50°C, the sensor utilizes LEDs with an operating wavelength of around 1660 nm. The system employs two optically filtered detectors and stabilizes the temperatures of the source and detectors. Vargas-Rodríguez and Rutt (2009) further exemplify opto-pair sensors operating in the 3.5 μm wavelength region, using InAsSb(P)- and InGaAs(Sb)-based LEDs as radiation sources. These novel analyzers offer small, responsive, and energy-efficient advantages. Previous non-dispersive optical techniques for methane detection relied on narrowband interference filters to

absorb infrared light in the 3.2–3.4 or 1.65–1.67 μm bands (Kwaśny & Bombalska, 2023). Instruments relying on photoacoustic conditions or opto-pairs can detect the presence of additional hydrocarbons. Moreover, an optical correlator mimicking the features of gas absorption lines can provide substantially higher selectivity for methane determination.

Raman Spectroscopy

Raman spectroscopy, a non-destructive method, can characterize methane, even when dissolved in salty water samples, as demonstrated by Caumon et al. (2014). They utilize novel high-pressure optic cells with capillaries made of fused silicon, depicted in Figure 11. The system works by modifying the external pressure in capillaries in order to capture methane internally. Raman spectroscopy, a vibrational spectroscopic technique, offers insight into the chemical composition of gases, molecular interactions, and structure (Kamieniak et al., 2015). Similar to infrared spectroscopy, Raman spectroscopy focuses an electromagnetic radiation beam on a sample, which interacts with specific molecular vibrational modes. Unlike infrared spectroscopy, Raman spectroscopy allows for a wider range of laser wavelengths, resulting in the observable Raman Effect, characteristic of inelastic light scattering processes such as the Stokes or anti-Stokes shift. In the anti-Stokes shift, the laser stimulates a molecular structure from a vibrating state, and after light scattering, it returns to its ground state. In the Stokes shift, a molecular structure is stimulated from its ground state after light scattering and returns to a vibrating state. Since the 1930s, Raman spectroscopy has been utilized to describe compounds inorganic and organic. According to Hansuld and Briens (2014), the primary advantage of this approach is its extremely high spatial resolution and minimal sample preparation requirements. Despite each molecule having a distinct set of molecular bonds, the Raman spectrum can be used to identify the molecular signature of each molecule.

Vibrational coherent anti-Stokes Raman spectroscopy is commonly employed for methane detection (Kamieniak et al., 2015). This technique involves irradiating the sample with two powerful laser beams at different frequencies, causing medium-frequency waves to mix and polarize, resulting in a signal laser beam. This method can measure the temperature and relative concentration ratio of CH_4 to N_2 in fuel-rich CH_4 air. Coherent anti-Stokes Raman spectroscopy focuses on vibrations within molecules by using numerous photons, producing an appropriate signal superior to that of standard Raman spectroscopy. Compared to spontaneous Raman, the resulting CARS spectrum offers substantially larger peak magnitudes (Bito et al., 2013). The primary benefits of this approach include high time, spectral, and spatial resolutions. However, a drawback of CARS is that it requires the initiation of the process, as the anti-Stokes situation results in a less energetically favorable final vibrational state, causing the released photons to have a higher frequency and be in an excited state (Hansuld & Briens, 2014; Schlücker, 2014).

Methane dissolved in water exhibits two significantly weaker bands at 3017 cm^{-1} and 3066 cm^{-1}, along with a stretched vibrational peak at approximately 2915 cm^{-1} (Hester et al., 2007). The key limitation of this method is the dimensions and cost of equipment. Due to its large size and permanent connections, the equipment is typically used in laboratories and cannot be transported to the field. Therefore, this method is not suitable for online measurements in the industry. Further research into handheld Raman devices for gaseous samples is needed if this technology is to be used in the field.

Raman spectroscopy, a non-destructive method, can characterize methane, even when dissolved in salty water samples, as demonstrated by Caumon et al. (2014). They utilize novel high-pressure optical cells with capillaries made of fused silicon, depicted in Figure 11. The system works by modifying the external pressure in capillaries to capture methane internally.

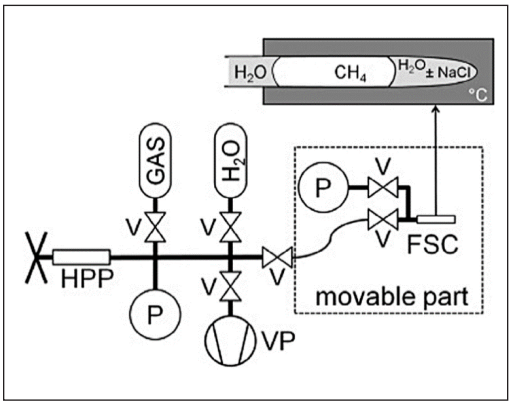

Figure 11. Optical cells under high pressure are utilized (Caumon et al., 2014). Here, FSC stands for fused-silica capillary, HPP for high-pressure pump, V for valve, P for pressure transducer, and VP for vacuum pump

Surface Plasmon Resonance

A sensor based on surface plasmon generation is known as a plasmonic sensor. Surface plasmons are a sort of light that occurs at a metal-dielectric interaction when incident radiation excites electrons, generating an electric field that propagates along the metal surface (Allsop & Neal, 2021). The parameters influencing spectrum behavior, optical properties, and surface plasmon sensing capabilities include the refracting index of metal, thickness, surface roughness, topology, extinction coefficient, and the surrounding refracting index, which forms an interface (Homola & Piliarik, 2006). These different scenarios lead to various types of surface plasmon processes.

By focusing on an optical instance, surface plasmon resonance (SPR) is triggered at the metal-dielectric connection by a diagonal magnetically polarized light source, known as surface plasmon waves (SPWs). A noteworthy decrease in the intensity of light reflection occurs due to the significance in absorption caused by the excitation of SPWs when the energy of the incident light coincides with that of SPW (Figure 12).

The study of sensitive NIR absorbance sensing tools with improved selectivity over traditional IR absorbance sensors involves a method recognized as surface-enhanced infrared resonant absorption spectroscopy. This method entails fine-tuning the SPR peak to align with the vibrating band of CH_4 molecules at the NIR wavelength (Abb et

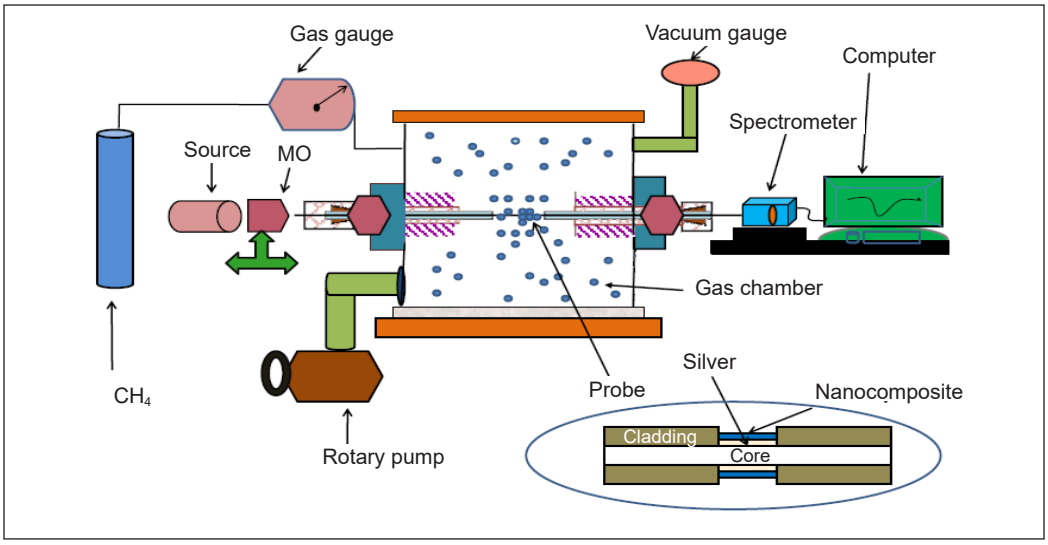

Figure 12. Schematic illustration of the SPR sensor used to detect methane gas (Mishra et al., 2015)

al., 2014). Recent examples include ITO nanocrystals (Kim et al., 2015). An equivalent strategy may be employed for CH_4 sensing, where the CO_2 characteristic band could be matched by adjusting the plasmon absorption strength via the Sn doping ratio. Additionally, including nanoparticles (AuNP) introduces a distinct type of surface plasmon resonance in metallic oxide-related detecting surfaces, particularly for high-temperature optical sensors (Ohodnicki et al., 2014). Furthermore, when exposed to CH_4, metal oxides can directly alter the optical absorbance of the metal oxide layer (Kamal et al., 2021).

Cavity Ring-down Spectroscopy

Cavity ring-down absorption spectroscopy (CRDS) technology was pioneered in 1988. Since then, a wide range of experimental modifications to CRDS spectroscopy have been developed, particularly over the last decade (Paldus & Kachanov, 2005). Foltynowicz et al. (2008) have comprehensively reviewed cavity-enhanced methods and their comparative efficacy. CRDS has become a popular method for analyzing the optical absorbance of atoms, particles, and infrared substances.

Continuous wave CRDS has been employed to investigate C–H overtone absorptions in methane, particularly focusing on wavelengths around 1.3 µm, using a slit jet expansion technique (Hippler & Quack, 2002). Research within this wavelength range has also been conducted under low-pressure and room-temperature conditions. While measurements of the absorption cross section ($\boldsymbol{\sigma}$) strongly correlate with earlier spectroscopic findings, the detection limits are less favorable in the shorter wavelength band. It is attributed to the significantly lower magnitudes of $\boldsymbol{\sigma}$ observed at wavelengths near 1.33 µm compared to the CH_4 $2v_3$ overtone absorption band at 1.66 µm (Fawcett et al., 2002).

The CRDS approach relies on determining the duration for which radiation remains trapped within an optical resonator. This resonator typically consists of two highly reflective mirrors (R > 99.995%). When a pulsed laser beam, lasting approximately 50 ns, is presented into the cavities, each mirror reflection results in a fraction (1- R) of the circulating radiation being released. In contrast, the remaining portion is mirrored again into the cavity. Figure 13 illustrates the operational mechanism of the CRDS method.

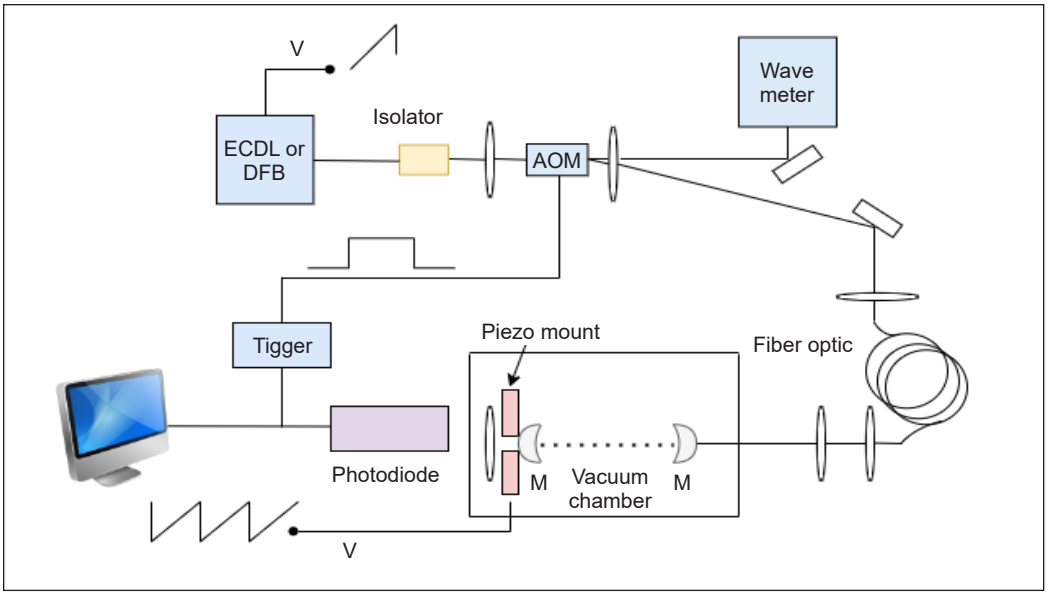

Figure 13. Illustration of Cavity Ring-Down Spectroscopy method. Here, AOM is an acoustic optic modulator; DFB is a distributed feedback laser; M is a mirror; and ECDL is an external cavity diode laser

A photomultiplier tube is employed for radiation detection behind the output mirror, while a digital oscilloscope monitors the output signal. When the cavity is filled with an absorbing substance, and the laser pulse reaches the wavelength of the absorbing gas, its decay time is reduced. Initially, the radiation decay time is determined with the empty cavity, and after that, the measurement is repeated with the addition of an absorber. Equation 4 expresses the time when the radiation (t) in the cavity disappears (Kwaśny & Bombalska, 2023).

$$\tau = \frac{L}{c[1-R) + \alpha L]} \quad [4]$$

Where L is the cavity length, R is the mirror's reflectance, and α is the coefficient of absorption.

Many CRDS method variants have been employed to find methane with ppb sensitivity (Lang et al., 2016). Numerous CRDS strategies are being used nowadays. Table 5 lists the most widely used CRDS approaches.

Table 5
Mostly used CRDS techniques

Method	Elements	Reference
Pulsed CRDS	Laser pulses are employed	He & Orr, 2000
Continuous Wave CRDS	Continuous action lasers	Romanini et al., 1997
Cavity Enhanced Absorption Spectroscopy	Consists of inserting a beam of radiation into the optical cavity off-axis	Pipino, 1999
Evanescent CRDS	Makes use of the vanishing wave principle	Atherton et al., 2004
Ring-Down Spectral Photography	With spectral decay photography	Hamilton & Orr-Ewing, 2011

COMPARISON OF PERFORMANCES

Table 6 summarizes the performance characteristics of the optical fiber instruments utilized for methane detection. The comparison of various optical fiber sensors for methane detection reveals significant differences in their performance, sensitivity, detection limits, and response times. The SnO_2/Graphene offers a broad detection range of 0 to 55%, with a detection limit of approximately 1.0%. However, the table does not mention any specific remarks or response times for this sensor, leaving questions about its practicality for real-time applications.

Table 6
Overview of the several types of optical fiber sensors used to detect methane (Adapted from Allsop & Neal, 2021)

Substance for discerning perception	Sensitivity (nm/%)	Detection limit (%)	Range (%)	Remarks	Reference
SnO_2/Graphene	-	~ 1.0	0 – 55	Not stated	Zhang et al., 2017
Pt/ZnO	0.01	~ 0.15	0 – 100	Regeneration, 1 s of response time	Allsop et al., 2018
Graphene+Ag	0.34	~ 0.1	0 – 3.5	Regeneration, 50 s and 160 s of response time	Wei et al., 2016
Graphene+CNTs and PMMA	1000	~ 0.0007	0 –0.01	Not stated	Mishra et al., 2015
Crytophane A	-1.99	~ 0.2	0 – 3.5	Not stated	Liu et al., 2018
Crytophane A	2.5	~ 0.2	0 – 3.5	Regeneration, 60 s and 180 s of response time	Yang et al., 2017
Crytophane A	6.39	~ 0.015	0 – 3.5	Not stated	Liu et al., 2019
Crytophane E	1.272	~ 0.02	0 – 5	Not stated	Wang et al., 2021
Crytophane E	4.6	~ 0.04	0 – 3	Regeneration, 60 s and 180 s of response time	Liu et al., 2020
Crytophane E	- 1.6	~ 0.06	0 – 5	5 min of response time	Zhang et al., 2015

In contrast, the Pt/ZnO sensor provides a sensitivity of 0.01 nm/% and a detection limit of 0.15%, covering a wide operational range from 0 to 100%. Notably, it features fast regeneration with a response time of just one second, making it ideal for scenarios requiring immediate feedback. The Graphene + Ag offers moderate sensitivity at 0.34 nm/% with a detection limit of around 0.1%, but it operates within a narrower range of 0 to 3.5%. It supports regeneration but with longer response times of 50 to 160 s, making it less suitable for applications needing rapid response.

The Graphene + CNTs with PMMA sensor stands out with the highest sensitivity in the group, at 1000 nm/%, and a detection limit as low as 0.0007%. However, this sensor's operational range is extremely limited, from 0 to 0.01%, making it more appropriate for detecting trace-level methane concentrations. The performance of Crytophane A varies significantly across studies, with sensitivity ranging from -1.99 to 6.39 nm/% and detection limits between 0.015% and 0.2%. Its operational range is generally constrained to 0 to 3.5%. Some variants, like the one reported by Yang et al. (2017), feature regeneration with response times of 60 to 180 s, making it suitable for continuous monitoring with moderate sensitivity.

The Crytophane E sensors also exhibit diverse performance metrics, with sensitivity ranging from -1.6 to 4.6 nm/% and detection limits between 0.02% and 0.06%. Their operational ranges vary from 0 to 3% or 0 to 5%, depending on the specific study. While one version (Liu et al., 2020) offers regeneration with response times of 60 to 180 s, another (Zhang et al., 2015) demonstrates a much longer response time of five minutes, suggesting variability in recovery efficiency.

In summary, each sensor presents trade-offs between sensitivity, range, and response time. The Graphene + CNTs with PMMA sensor excels in detecting very low methane concentrations but is limited by its narrow range. Pt/ZnO offers the fastest response and widest range, making it ideal for dynamic environments. Meanwhile, Crytophane A and Crytophane E provide moderate sensitivity with some variants supporting regeneration, though their response times vary significantly. These insights suggest that selecting the appropriate sensor depends on the specific requirements of the application, such as detection precision, response speed, or operational range.

RECENT RESEARCH DEVELOPMENTS OF OPTICAL SENSORS

Several studies have focused on improving optical methane sensors. In recent years, infrared methane detection technology has gained popularity due to its numerous advantages, including longevity, high reliability, wide applicability, and precise detection capabilities (Yu et al., 2014). Among various laser-based methane detection techniques, photoacoustic spectroscopy has emerged as particularly promising. It has demonstrated its ability, more effectively than established methods such as Cavity Ring-down spectroscopy, differential

spectroscopy, or higher-frequency modulation techniques, to serve several distinct applications such as commercial surveillance, healthcare (e.g., breath analysis for disease diagnosis), and atmospheric and ecological studies. An optical correlator that matches gas absorption lines offers significantly improved selectivity for methane detection. In optical gas sensors that utilize laser absorption spectroscopy, photoacoustic spectroscopy, optical resonators (cavities), and multi-pass gas cells are foundational components (Mikołajczyk et al., 2016). TDLAS stands out as the most advanced, versatile, and efficient optical technique for gas detection (McManus, 2010). This method enables both in-person and remote measurements to be conducted.

Iseki et al. (2000) developed a compact remote methane sensor utilizing a 1.65 μm InGaAsP distributed feedback laser. It is intended to be a man-portable, long-path absorbance lidar that can reach up to 10 meters using a topographical target. Scanning the laser light is a simple way for an operator to look for gas leaks. Dong et al. (2007) proposed a cavity-enhanced method for a Fabry-Pérot cavity (FPC) sensor to increase the precision of gas measurements. The method comprised scanning the cavity length at each laser frequency to record the transmission maxima of the cavity modes. After integrating the new approach, it was discovered that the FPC sensor could detect methane with a sensitivity of 0.7–2.9 parts per million by mass (ppm-m).

An optical fiber-based methane sensor based on stannic oxide doped with graphene was studied by Zhang et al. (2017). Thin graphene-doped tin oxide coatings were put on side-polished optical fibers to create the sensor, and a wavelength of 1550 nm was chosen as the optical spectrum's light source. The optical fibers' output light intensities were measured using various methane concentrations. The refractive index and SnO_2 conductivity rose in parallel with the methane concentration. As a result, the absorption coefficient dropped, and the output light intensity improved. The results demonstrated that adding graphene-doped SnO_2 enhanced the sensor's sensitivity, repeatability, output light intensity, and dependability.

Tombez et al. (2017) developed a tiny, affordable, and IR-adjustable diode-laser absorption spectroscope with silicon at chip-scale photonics integrated for flexible gas sensors. With an uncooled InGaAs detection technique equipped with a high-contrast index silicon waveguide at the nanoscale, the authors analyzed ambient methane using near-IR (1650 nm) light from a laser with distributed feedback, achieving a sub-100 ppm-v limit of detection. An easy, inexpensive, and modest all-fiber methane sensor was created by Ismaeel et al. (2019). It is made up of two fiber Bragg gratings and an optical fiber with a D-shaped cross-section. The Teflon layer covering the fiber was the most important development in this work, which was doped with cryptophane, a substance that prefers methane gas. With a reaction time of 4 s, the sensor reached an impressive sensitivity (0.16 nm/ppm-m).

Recently, there has been a study on a potential technology called hollow-core photonic crystal fiber, where a more effective light-gas interaction is made possible by the gas being firmly filled into the hollow core (Xie et al., 2016). HC-PBF-based photothermal spectroscopy enables the detection of various gases, including CH_4, H_2S, CO_2, CO, and NH_3, among others. However, it is worth noting that the length of the HC-PBF can influence the sensor's sensitivity and reaction time. Additionally, a recent development involves utilizing UAVs with remotely operated methane detectors, offering a promising solution for detecting natural gas leakage in pipelines (Hollenbeck et al., 2021).

COMMERCIAL APPLICATIONS OF OPTICAL-BASED METHANE SENSORS

Optical fiber-based methane sensors have become increasingly popular due to their high sensitivity, fast response times, and immunity to electromagnetic interference. These sensors capitalize on the interaction between methane molecules and light traveling through optical fibers, providing benefits such as remote sensing, multiplexing, and suitability for challenging environments. This review delves into the practical applications of optical fiber-based methane sensors in commercial settings, showcasing their versatility across different industries. It also underscores recent sensor design and performance innovations, demonstrating the ongoing advancements in this field.

In the oil and gas sector, optical fiber-based methane sensors have emerged as valuable tools for leak detection and emissions monitoring in upstream, midstream, and downstream operations. According to Collins et al. (2022), distributed optical fiber sensors enable continuous monitoring of methane concentrations along pipelines and wellheads, providing real-time data for early leak detection and localization. Integrating optical fibers into existing infrastructure offers a cost-effective solution for enhancing safety protocols and minimizing environmental impact.

Environmental monitoring applications of optical fiber-based methane sensors encompass a wide range of scenarios, including landfill gas management, agricultural emissions, and ecosystem research. As highlighted by Butt et al. (2022), distributed optical fiber sensing technology enables spatially resolved monitoring of methane emissions from landfills, facilitating the optimization of gas collection systems and the assessment of emission mitigation strategies. Similarly, optical fiber-based sensors provide valuable insights into methane production from livestock activities and manure management practices in agricultural settings.

Optical fiber-based methane sensors also find applications in industrial process control and quality assurance, particularly in chemical synthesis, fermentation, and biogas production processes. Fiber-optic sensing platforms offer high sensitivity and multiplexing capabilities, enabling real-time monitoring of methane concentrations in reactors and

bioreactors. They facilitate process optimization, yield maximization, and product quality assurance, contributing to operational efficiency and cost savings in industrial manufacturing.

The commercialization of optical fiber-based methane sensors is poised for continued growth, driven by advancements in sensor technology, miniaturization, and integration with data analytics platforms. Moreover, integrating optical fiber sensing networks with artificial intelligence algorithms holds promise for autonomous monitoring systems and predictive maintenance strategies, opening new avenues for commercial applications in smart cities, industrial automation, and environmental monitoring.

CONCLUSION

This study has reviewed recent advancements in optical-based techniques for methane detection. Detecting even the smallest methane leaks is highlighted due to the potential explosions and environmental impact risks. Spectroscopic methods can provide both qualitative and quantitative assessments of methane levels. In addition, highly specific and sensitive methodologies are available, enabling accurate determination of methane concentrations. Unfortunately, the available spectroscopic instruments are primarily designed for laboratory use, resulting in higher operational costs and limited suitability for point-of-care analysis. Additionally, these instruments are not conducive to real-time monitoring. Given the escalating concerns regarding greenhouse gas emissions, industries must accurately track the temporal variations in methane concentrations to gain comprehensive insights into these emissions. A reliable, real-time measurement system is imperative for facilitating efficient management of greenhouse gas emissions and establishing a responsive underground mine ventilation system.

Nonetheless, Tunable Diode Laser Absorption Spectroscopy (TDLAS) emerges as a portable spectroscopic technique that can be deployed directly at the site of environmental pollution. TDLAS is further enhanced through its integration with fiber optics, enabling distributed sensing and monitoring of diverse gases. It includes open paths, gas cells, evanescent fields, and microstructure fiber-optic sensors. Optical fiber-based methane measurement stands out as a unique approach for sensing methane gas concentrations, particularly in industrial settings such as the mining sector.

Moreover, current techniques either require human intervention or exhibit significant time delays in accurately measuring gas concentrations within the target area. Future research endeavors in distributed optical fiber-based sensing techniques, particularly those employing sequential multi-cells, should prioritize developing and evaluating resilient and effective gas sensors capable of accurately measuring gas concentrations in challenging environments.

ACKNOWLEDGMENTS

The authors sincerely thank the Universiti Malaysia Pahang Al-Sultan Abdullah (UMPSA), Malaysia, for supporting and providing research funds for this project (PDU233203). Additionally, the authors would like to sincerely thank the Faculty of Electrical and Electronics Engineering Technology, UMPSA, Malaysia, for providing access to a few facilities.

REFERENCES

Abb, M., Wang, Y., Papasimakis, N., De Groot, C. H., & Muskens, O. L. (2014). Surface-enhanced infrared spectroscopy using metal oxide plasmonic antenna arrays. *Nano Letters*, *14*(1), 346–352. https://doi.org/10.1021/nl404115g

Agius, C., Brenon, M., Dill, W. G., Kelly, P., Klausmeyer, U., McManama, K., Pogorelsky, A., & Zalogine, A. S. (2000). The impact of the IECEx scheme on the global availability of explosion protected apparatus-update 2000 (parts IV-VII). In *Conference Record of the 2000 IEEE Industry Applications Conference. Thirty-Fifth IAS Annual Meeting and World Conference on Industrial Applications of Electrical Energy (Cat. No. 00CH37129)* (Vol. 4, pp. 2844-2851). IEEE Publishing. https://doi.org/10.1109/IAS.2000.883225

Allsop, T., & Neal, R. (2021). A review: Application and implementation of optic fibre sensors for gas detection. *Sensors*, *21*(20), Article 6755. https://doi.org/10.3390/s21206755

Allsop, T., Kundrat, V., Kalli, K., Lee, G. B., Neal, R., Bond, P., Shi, B., Sullivan, J., Culverhouse, P., & Webb, D. J. (2018). Methane detection scheme based upon the changing optical constants of a zinc oxide/platinum matrix created by a redox reaction and their effect upon surface plasmons. *Sensors and Actuators B: Chemical*, *255*, 843–853. https://doi.org/10.1016/j.snb.2017.08.058

Atherton, K., Yu, H., Stewart, G., & Culshaw, B. (2004). Gas detection with fibre amplifiers by intra-cavity and cavity ring-down absorption. *Measurement Science and Technology*, *15*, 1621–1628.

Bachu, S. (2017). Analysis of gas leakage occurrence along wells in Alberta, Canada, from a GHG perspective – Gas migration outside well casing. *International Journal of Greenhouse Gas Control*, *61*, 146–154. https://doi.org/10.1016/j.ijggc.2017.04.003

Beckwith, P. H., Brown, C. E., Danagher, D. J., Smith, D. R., & Reid, J. (1987). High sensitivity detection of transient infrared absorption using tunable diode lasers. *Applied Optics*, *26*(13), Article 2643. https://doi.org/10.1364/AO.26.002643

Bito, K., Okuno, M., Kano, H., Leproux, P., Couderc, V., & Hamaguchi, H. (2013). Three-pulse multiplex coherent anti-Stokes/Stokes Raman scattering (CARS/CSRS) microspectroscopy using a white-light laser source. *Chemical Physics*, *419*, 156–162. https://doi.org/10.1016/j.chemphys.2013.02.007

Butt, M. A., Voronkov, G. S., Grakhova, E. P., Kutluyarov, R. V., Kazanskiy, N. L., & Khonina, S. N. (2022). Environmental monitoring: A comprehensive review on optical waveguide and fiber-based sensors. *Biosensors, 12*(11), Article 1038. https://doi.org/10.3390/bios12111038

Caumon, M. C., Robert, P., Laverret, E., Tarantola, A., Randi, A., Pironon, J., Dubessy, J., & Girard, J. P. (2014). Determination of methane content in NaCl–H_2O fluid inclusions by Raman spectroscopy. Calibration and application to the external part of the Central Alps (Switzerland). *Chemical Geology*, *378–379*, 52–61. https://doi.org/10.1016/j.chemgeo.2014.03.016

Collins, W., Orbach, R., Bailey, M., Biraud, S., Coddington, I., DiCarlo, D., Peischl, J., Radhakrishnan, A., & Schimel, D. (2022). Monitoring methane emissions from oil and gas operations. *Optics Express, 30*(14), Article 24326. https://doi.org/10.1364/OE.464421

Dong, L., Yin, W., Ma, W., Zhang, L., & Jia, S. (2007). High-sensitivity, large dynamic range, auto-calibration methane optical sensor using a short confocal Fabry–Perot cavity. *Sensors and Actuators B: Chemical*, *127*(2), 350–357. https://doi.org/10.1016/j.snb.2007.04.030

Fawcett, B. L., Parkes, A. M., Shallcross, D. E., & Orr-Ewing, A. J. (2002). Trace detection of methane using continuous wave cavity ring-down spectroscopy at 1.65 μm. *Physical Chemistry Chemical Physics, 4*(24), 5960–5965. https://doi.org/10.1039/B208486B

Foltynowicz, A., Schmidt, F. M., Ma, W., & Axner, O. (2008). Noise-immune cavity-enhanced optical heterodyne molecular spectroscopy: Current status and future potential. *Applied Physics B*, *92*(3), Article 313. https://doi.org/10.1007/s00340-008-3126-z

Formisano, V., Atreya, S., Encrenaz, T., Ignatiev, N., & Giuranna, M. (2004). Detection of methane in the atmosphere of Mars. *Science*, *306*(5702), 1758–1761. https://doi.org/10.1126/science.1101732

Gao, Q., Zhang, Y., Yu, J., Wu, S., Zhang, Z., Zheng, F., Lou, X., & Guo, W. (2013). Tunable multi-mode diode laser absorption spectroscopy for methane detection. *Sensors and Actuators A: Physical*, *199*, 106–110. https://doi.org/10.1016/j.sna.2013.05.012

Gardiner, T., Mead, M. I., Garcelon, S., Robinson, R., Swann, N., Hansford, G. M., Woods, P. T., & Jones, R. L. (2010). A lightweight near-infrared spectrometer for the detection of trace atmospheric species. *Review of Scientific Instruments*, *81*(8), Article 083102. https://doi.org/10.1063/1.3455827

Gurlit, W., Zimmermann, R., Giesemann, C., Fernholz, T., Ebert, V., Wolfrum, J., Platt, U., & Burrows, J. P. (2005). Lightweight diode laser spectrometer CHILD (Compact High-altitude In-situ Laser Diode) for balloonborne measurements of water vapor and methane. *Applied Optics, 44*(1), Article 91. https://doi.org/10.1364/AO.44.000091

Hamilton, D. J., & Orr-Ewing, A. J. (2011). A quantum cascade laser-based optical feedback cavity-enhanced absorption spectrometer for the simultaneous measurement of CH_4 and N_2O in air. *Applied Physics B*, *102*(4), 879–890. https://doi.org/10.1007/s00340-010-4259-4

Hansuld, E. M., & Briens, L. (2014). A review of monitoring methods for pharmaceutical wet granulation. *International Journal of Pharmaceutics*, *472*(1–2), 192–201. https://doi.org/10.1016/j.ijpharm.2014.06.027

He, Y., & Orr, B. J. (2000). Ringdown and cavity-enhanced absorption spectroscopy using a continuous-wave tunable diode laser and a rapidly swept optical cavity. *Chemical Physics Letters*, *319*(1–2), 131–137. https://doi.org/10.1016/S0009-2614(00)00107-X

Hennig, O., Strzoda, R., Mágori, E., Chemisky, E., Tump, C., Fleischer, M., Meixner, H., & Eisele, I. (2003). Hand-held unit for simultaneous detection of methane and ethane based on NIR-absorption

spectroscopy. *Sensors and Actuators B: Chemical, 95*(1–3), 151–156. https://doi.org/10.1016/S0925-4005(03)00399-X

Hester, K. C., Dunk, R. M., White, S. N., Brewer, P. G., Peltzer, E. T., & Sloan, E. D. (2007). Gas hydrate measurements at Hydrate Ridge using Raman spectroscopy. *Geochimica et Cosmochimica Acta*, *71*(12), 2947–2959. https://doi.org/10.1016/j.gca.2007.03.032

Hippler, M., & Quack, M. (2002). High-resolution Fourier transform infrared and cw-diode laser cavity ringdown spectroscopy of the v2+2v3 band of methane near 7510 cm−1 in slit jet expansions and at room temperature. *The Journal of Chemical Physics*, *116*(14), 6045–6055. https://doi.org/10.1063/1.1433505

Hodgkinson, J., & Pride, R. D. (2010). Methane-specific gas detectors: The effect of natural gas composition. *Measurement Science and Technology*, *21*(10), Article 105103. https://doi.org/10.1088/0957-0233/21/10/105103

Hodgkinson, J., & Tatam, R. P. (2013). Optical gas sensing: A review. *Measurement Science and Technology*, *24*(1), Article 012004. https://doi.org/10.1088/0957-0233/24/1/012004

Hodgkinson, J., Shan, Q., & Pride, R. D. (2006). Detection of a simulated gas leak in a wind tunnel. *Measurement Science and Technology*, *17*(6), 1586–1593. https://doi.org/10.1088/0957-0233/17/6/041

Hollenbeck, D., Zulevic, D., & Chen, Y. (2021). Advanced leak detection and quantification of methane emissions using sUAS. *Drones*, *5*(4), Article 117. https://doi.org/10.3390/drones5040117

Homola, J., & Piliarik, M. (2006). *Surface Plasmon Resonance (SPR) sensors*. Springer.

Hong, T., Culp, J. T., Kim, K. J., Devkota, J., Sun, C., & Ohodnicki, P. R. (2020). State-of-the-art of methane sensing materials: A review and perspectives. *TrAC Trends in Analytical Chemistry*, *125*, Article 115820. https://doi.org/10.1016/j.trac.2020.115820

Ingraffea, A. R., Wawrzynek, P. A., Santoro, R., & Wells, M. (2020). Reported methane emissions from active oil and gas wells in Pennsylvania, 2014–2018. *Environmental Science & Technology*, *54*(9), 5783–5789. https://doi.org/10.1021/acs.est.0c00863

Iseki, T., Tai, H., & Kimura, K. (2000). A portable remote methane sensor using a tunable diode laser. *Measurement Science and Technology*, *11*(6), 594–602. https://doi.org/10.1088/0957-0233/11/6/302

Ismaeel, R., Beaton, A., Donko, A., Talataisong, W., Lee, T., Brotin, T., Beresna, M., Mowlem, M., & Brambilla, G. (2019). High sensitivity all-fibre methane sensor with gas permeable teflon/cryptophane-a membrane. In *The European Conference on Lasers and Electro-Optics* (p. ch_6_5). Optica Publishing Group.

Jaramillo, P., Griffin, W. M., & Matthews, H. S. (2008). Comparative analysis of the production costs and life-cycle GHG emissions of FT liquid fuels from coal and natural gas. *Environmental Science & Technology*, *42*(20), 7559–7565. https://doi.org/10.1021/es8002074

Kamal, D. A. M., Ibrahim, S. F., Kamal, H., Kashim, M. I. A. M., & Mokhtar, M. H. (2021). Physicochemical and medicinal properties of Tualang, Gelam and Kelulut Honeys: A comprehensive review. *Nutrients*, *13*(1), Article 197. https://doi.org/10.3390/nu13010197

Kamieniak, J., Randviir, E. P., & Banks, C. E. (2015). The latest developments in the analytical sensing of methane. *TrAC Trends in Analytical Chemistry, 73,* 146–157. https://doi.org/10.1016/j.trac.2015.04.030

Kannath, A., Hodgkinson, J., Gillard, R. G., Riley, R. J., & Tatam, R. P. (2011). A VCSEL based system for on-site monitoring of low level methane emission. In *Vertical-Cavity Surface-Emitting Lasers XV* (Vol. 7952, pp. 99-107). SPIE. https://doi.org/10.1117/12.874513

Kim, K. J., Chong, X., Kreider, P. B., Ma, G., Ohodnicki, P. R., Baltrus, J. P., Wang, A. X., & Chang, C. H. (2015). Plasmonics-enhanced metal–organic framework nanoporous films for highly sensitive near-infrared absorption. *Journal of Materials Chemistry C*, *3*(12), 2763–2767. https://doi.org/10.1039/C4TC02846E

Kwaśny, M., & Bombalska, A. (2023). Optical methods of methane detection. *Sensors*, *23*(5), Article 2834. https://doi.org/10.3390/s23052834

Lang, N., Macherius, U., Wiese, M., Zimmermann, H., Röpcke, J., & Van Helden, J. H. (2016). Sensitive CH_4 detection applying quantum cascade laser based optical feedback cavity-enhanced absorption spectroscopy. *Optics Express*, *24*(6), Article A536. https://doi.org/10.1364/OE.24.00A536

Lawrence, N. (2006). Analytical detection methodologies for methane and related hydrocarbons. *Talanta*, *69*(2), 385–392. https://doi.org/10.1016/j.talanta.2005.10.005

Liu, H., Wang, H., Chen, C., Zhang, W., Bai, B., Chen, C., Zhang, Y., & Shao, Q. (2020). High sensitive methane sensor based on twin-core photonic crystal fiber with compound film-coated side-holes. *Optical and Quantum Electronics*, *52*(2), Article 81. https://doi.org/10.1007/s11082-020-2198-9

Liu, H., Wang, M., Wang, Q., Li, H., Ding, Y., & Zhu, C. (2018). Simultaneous measurement of hydrogen and methane based on PCF-SPR structure with compound film-coated side-holes. *Optical Fiber Technology*, *45*, 1–7. https://doi.org/10.1016/j.yofte.2018.05.007

Liu, H., Zhang, Y., Chen, C., Bai, B., Shao, Q., Wang, H., Zhang, W., Chen, C., & Tang, S. (2019). Transverse-stress compensated methane sensor based on long-period grating in photonic crystal fiber. *IEEE Access*, *7*, 175522–175530. https://doi.org/10.1109/ACCESS.2019.2951133

McDermitt, D., Burba, G., Xu, L., Anderson, T., Komissarov, A., Riensche, B., Schedlbauer, J., Starr, G., Zona, D., Oechel, W., Oberbauer, S., & Hastings, S. (2011). A new low-power, open-path instrument for measuring methane flux by eddy covariance. *Applied Physics B*, *102*(2), 391–405. https://doi.org/10.1007/s00340-010-4307-0

McManus, J. B. (2010). Application of quantum cascade lasers to high-precision atmospheric trace gas measurements. *Optical Engineering*, *49*(11), Article 111124. https://doi.org/10.1117/1.3498782

McManus, J. B., Shorter, J. H., Nelson, D. D., Zahniser, M. S., Glenn, D. E., & McGovern, R. M. (2008). Pulsed quantum cascade laser instrument with compact design for rapid, high sensitivity measurements of trace gases in air. *Applied Physics B, 92*(3), Article 387. https://doi.org/10.1007/s00340-008-3129-9

Mikołajczyk, J., Wojtas, J., Bielecki, Z., Stacewicz, T., Szabra, D., Magryta, P., Prokopiuk, A., Tkacz, A., & Panek, M. (2016). System of optoelectronic sensors for breath analysis. *Metrology and Measurement Systems*, *23*(3), 481–489. https://doi.org/10.1515/mms-2016-0030

Mishra, S. K., Tripathi, S. N., Choudhary, V., & Gupta, B. D. (2015). Surface plasmon resonance-based fiber optic methane gas sensor utilizing graphene-carbon nanotubes-poly(methyl methacrylate) hybrid nanocomposite. *Plasmonics*, *10*(5), 1147–1157. https://doi.org/10.1007/s11468-015-9914-5

Ohodnicki Jr., P. R., Brown, T. D., Holcomb, G. R., Tylczak, J., Schultz, A. M., & Baltrus, J. P. (2014). High temperature optical sensing of gas and temperature using AU-nanoparticle incorporated oxides. *Sensors and Actuators B: Chemical*, *202*, 489–499. https://doi.org/10.1016/j.snb.2014.04.106

Olmer, N., Comer, B., Roy, B., Mao, X., & Rutherford, D. (2019, November 25). *Greenhouse gas emissions from global shipping, 2013—2015 Detailed Methodology*. https://www.theicct.org/publications/GHG-emissions-globalshipping-2013-2015

Paldus, B. A., & Kachanov, A. A. (2005). An historical overview of cavity-enhanced methods. *Canadian Journal of Physics*, *83*(10), 975–999. https://doi.org/10.1139/p05-054

Pipino, A. C. R. (1999). Ultrasensitive surface spectroscopy with a miniature optical resonator. *Physical Review Letters*, *83*(15), 3093–3096. https://doi.org/10.1103/PhysRevLett.83.3093

Pyun, S. H., Cho, J., Davidson, D. F., & Hanson, R. K. (2011). Interference-free mid-IR laser absorption detection of methane. *Measurement Science and Technology*, *22*(2), Article 025303. https://doi.org/10.1088/0957-0233/22/2/025303

Richard, E. C., Kelly, K. K., Winkler, R. H., Wilson, R., Thompson, T. L., McLaughlin, R. J., Schmeltekopf, A. L., & Tuck, A. F. (2002). A fast-response near-infrared tunable diode laser absorption spectrometer for in situ measurements of CH 4 in the upper troposphere and lower stratosphere. *Applied Physics B: Lasers and Optics, 75*(2–3), 183–194. https://doi.org/10.1007/s00340-002-0935-3

Romanini, D., Kachanov, A. A., & Stoeckel, F. (1997). Diode laser cavity ring down spectroscopy. *Chemical Physics Letters*, *270*(5–6), 538–545. https://doi.org/10.1016/S0009-2614(97)00406-5

Rothman, L. S., Gordon, I. E., Barbe, A., Benner, D. C., Bernath, P. F., Birk, M., Boudon, V., Brown, L. R., Campargue, A., Champion, J.-P., Chance, K., Coudert, L. H., Dana, V., Devi, V. M., Fally, S., Flaud, J.-M., Gamache, R. R., Goldman, A., Jacquemart, D., … & Vander Auwera, J. (2009). The HITRAN 2008 molecular spectroscopic database. *Journal of Quantitative Spectroscopy and Radiative Transfer*, *110*(9–10), 533–572. https://doi.org/10.1016/j.jqsrt.2009.02.013

Schlücker, S. (2014). Surface-enhanced Raman spectroscopy: Concepts and chemical applications. *Angewandte Chemie International Edition*, *53*(19), 4756–4795. https://doi.org/10.1002/anie.201205748

Shao, L., Fang, B., Zheng, F., Qiu, X., He, Q., Wei, J., Li, C., & Zhao, W. (2019). Simultaneous detection of atmospheric CO and CH_4 based on TDLAS using a single 2.3 μm DFB laser. *Spectrochimica Acta Part A: Molecular and Biomolecular Spectroscopy, 222*, Article 117118. https://doi.org/10.1016/j.saa.2019.05.023

Shemshad, J., Aminossadati, S. M., & Kizil, M. S. (2012). A review of developments in near infrared methane detection based on tunable diode laser. *Sensors and Actuators B: Chemical*, *171–172*, 77–92. https://doi.org/10.1016/j.snb.2012.06.018

Stocker, T. F., Dahe, Q., Plattner, G. K., Tignor, M. B., Allen, S. K., Boschung, J., Nauels, A., Xia, Y., Bex, V., & Midgley, P. (2014). *Climate change 2013: The physical science basis*. Cambridge University Press.

Tiemann, M. (2007). Porous metal oxides as gas sensors. *Chemistry – A European Journal, 13*(30), 8376–8388. https://doi.org/10.1002/chem.200700927

Tombez, L., Zhang, E. J., Orcutt, J. S., Kamlapurkar, S., & Green, W. M. J. (2017). Methane absorption spectroscopy on a silicon photonic chip. *Optica*, *4*(11), Article 1322. https://doi.org/10.1364/OPTICA.4.001322

Tran, M. K., & Fowler, M. (2020). A review of lithium-ion battery fault diagnostic algorithms: Current progress and future challenges. *Algorithms*, *13*(3), Article 62. https://doi.org/10.3390/a13030062

Turner, A. J., Frankenberg, C., & Kort, E. A. (2019). Interpreting contemporary trends in atmospheric methane. *Proceedings of the National Academy of Sciences*, *116*(8), 2805–2813. https://doi.org/10.1073/pnas.1814297116

Vargas-Rodríguez, E., & Rutt, H. N. (2009). Design of CO, CO_2 and CH_4 gas sensors based on correlation spectroscopy using a Fabry–Perot interferometer. *Sensors and Actuators B: Chemical*, *137*(2), 410–419. https://doi.org/10.1016/j.snb.2009.01.013

Vasiliev, A. A., Pisliakov, A. V., Sokolov, A. V., Polovko, O. V., Samotaev, N. N., Kujawski, W., Rozicka, A., Guarnieri, V., & Lorencelli, L. (2014). Gas sensor system for the determination of methane in water. *Procedia Engineering*, *87*, 1445–1448. https://doi.org/10.1016/j.proeng.2014.11.721

Wang, X., & Wolfbeis, O. S. (2016). Fiber-optic chemical sensors and biosensors (2013–2015). *Analytical Chemistry*, *88*(1), 203–227. https://doi.org/10.1021/acs.analchem.5b04298

Wang, Z., Gao, P., Liu, S., & Chen, X. (2021). A reflective methane concentration sensor based on biconvex cone photonic crystal fiber. *Optik*, *241*, Article 166983. https://doi.org/10.1016/j.ijleo.2021.166983

Wei, T., Wu, H., Dong, L., Cui, R., & Jia, S. (2021). Palm-sized methane TDLAS sensor based on a mini-multi-pass cell and a quartz tuning fork as a thermal detector. *Optics Express, 29*(8), Article 12357. https://doi.org/10.1364/OE.423217

Wei, W., Nong, J., Zhang, G., Tang, L., Jiang, X., Chen, N., Luo, S., Lan, G., & Zhu, Y. (2016). Graphene-based long-period fiber grating surface plasmon resonance sensor for high-sensitivity gas sensing. *Sensors*, *17*(12), Article 2. https://doi.org/10.3390/s17010002

Wild, K. (2000). Gas quality measurement: A gas control revolution? *Gas Engineering and Management*, *40*, 12–14.

Wisen, J., Chesnaux, R., Werring, J., Wendling, G., Baudron, P., & Barbecot, F. (2020). A portrait of wellbore leakage in northeastern British Columbia, Canada. *Proceedings of the National Academy of Sciences*, *117*(2), 913–922. https://doi.org/10.1073/pnas.1817929116

Xie, S., Pennetta, R., & Russell, P. St. J. (2016). Self-alignment of glass fiber nanospike by optomechanical back-action in hollow-core photonic crystal fiber. *Optica*, *3*(3), Article 277. https://doi.org/10.1364/OPTICA.3.000277

Yang, J., Che, X., Shen, R., Wang, C., Li, X., & Chen, W. (2017). High-sensitivity photonic crystal fiber long-period grating methane sensor with cryptophane-A-6Me absorbed on a PAA-CNTs/PAH nanofilm. *Optics Express*, *25*(17), Article 20258. https://doi.org/10.1364/OE.25.020258

Yu, X., Lv, R. H., Song, F., Zheng, C. T., & Wang, Y. D. (2014). Pocket-sized nondispersive infrared methane detection device using two-parameter temperature compensation. *Spectroscopy Letters*, *47*(1), 30–37. https://doi.org/10.1080/00387010.2013.780082

Zhang, J. Y., Ding, E. J., Xu, S. C., Li, Z. H., Wang, X. X., & Song, F. (2017). Sensitization of an optical fiber methane sensor with graphene. *Optical Fiber Technology*, *37*, 26–29. https://doi.org/10.1016/j.yofte.2017.06.011

Zhang, Y., Zhao, Y., & Wang, Q. (2015). Measurement of methane concentration with cryptophane E infiltrated photonic crystal microcavity. *Sensors and Actuators B: Chemical*, *209*, 431–437. https://doi.org/10.1016/j.snb.2014.12.002